# A New Series of Chalcohalide Semiconductors with Composite $CdBr_2/Sb_2Se_3$ Lattices: Synthesis and Characterization of $CdSb_2Se_3Br_2$ and Indium Derivatives $InSb_2S_4X$ (X = Cl and Br) and $InM_2Se_4Br$ (M = Sb and Bi)

Lei Wang[†] and Shiou-Jyh Hwu*

*Department of Chemistry, Clemson University, Clemson, South Carolina 29634-0973*

*Received July 24, 2007. Revised Manuscript Received September 13, 2007*

A new series of mixed-framework compounds in the chalcohalide family has been synthesized using the conventional solid-state reactions. These include $CdSb_2Se_3Br_2$ **1** and its isoelectronic indium derivatives $InSb_2S_4X$ (X = Cl **2** and Br **3**) and $InM_2Se_4Br$ (M = Sb **4** and Bi **5**). Single crystals were grown from direct interaction of stoichiometric mixtures of respective elemental and binary compounds. The parent compound cadmium antimony selenobromide, $CdSb_2Se_3Br_2$, was synthesized by heating the stoichiometric mixture of $CdBr_2$ and Sb and Se at 450 °C followed by slow cooling. Single-crystal structure analysis was carried out by employing X-ray diffraction methods, showing that this compound crystallizes in the monoclinic crystal system (*C*2/*m*, No. 12) with $a = 20.998(4)$ Å, $b = 4.0260(8)$ Å, $c = 12.149(2)$ Å, $\beta = 119.00(3)°$, and $V = 898.3(3)$ Å$^3$. The framework exhibits mixed $CdBr_2$ and $Sb_2Se_3$ sublattices, respectively, adopting the (110) and (100) NaCl-type structures. The former consists of dual octahedral chains of Cd-centered [$CdBr_5Se$] units sharing *cis* Br edges, and the chains propagate along the *b* axis via sharing *trans* Br edges of the octahedra. The $Sb_2Se_3$ sublattice is made of three edge-shared [$SbSe_5$] square-pyramidal units, features commonly seen in antimony and Sb-containing selenides. The apex selenium atoms of the aforementioned [$CdBr_5Se$] unit are corner-shared with [$SbSe_5$] sublattices to form a composite slab along the (−101) plane. The lone-pair electrons of $Sb^{3+}$ cations point into the space between the stacked slabs. The indium derivatives **2**–**5** were synthesized by substituting the trivalent $In^{3+}$ for divalent $Cd^{2+}$ cations, along with a stoichiometric amount of charge-compensating halide anions. These four new In derivatives are isostructural with **1** and can be formulated as $(InSX)(Sb_2S_3)$ (X = Cl and Br), and $(InSeBr)(M_2Se_3)$ (M = Sb and Bi) with respect to the composite lattices of $CdBr_2$ and $Sb_2Se_3$. The UV–vis reflectance spectroscopy and band structure calculations confirm that these compounds are semiconductors with steep band gap absorption edges around 1.1–1.8 eV. In light of the observed blue shift in the absorption edge with respect to the dimensionally reduced post-transition-metal chalcogenide $M_2Q_3$ sublattices, we claim quantum confinement effect of the optical band gap, which is the first example among inorganic mixed-anion compounds reported thus far.

## Introduction

There is an extensive interest in exploring new low-dimensional materials because they often offer novel and enhanced physical properties of fundamental and technological interests. Inorganic/organic hybrid compounds, for example, are well-known for their unique structural and electronic properties,[1–3] such as porous solids made of metal organic framework (MOF),[1] layered perovskites engineered by organic-based metal halides,[2] and inorganic nanodots encapsulated by organic molecules.[3] While their reaction mechanism is not fully revealed, these classes of hybrid materials can be made in bulk quantity, which demonstrates the utility of organic molecules and their functional groups for the formation of low-dimensional structures of "controlled" size and geometry. By the same token, all-inorganic hybrid solids made of mixed magnetic/nonmagnetic frameworks, for instance, have been reported in oxide systems incorporating oxyanions. In $RE_4M(Si_2O_7)_2(MO_2)_{4m}$ (RE = La and Nd; M = Ti and V), where *m* represents the thickness of the electronically reduced $MO_2$ rutile layers, the silicate slabs function as spacers as well as linkers with respect to the formation of low-dimensional rutile layers.[4] These structurally isolated and electronically insulated magnetic lattices are of fundamental and technological importance

* To whom correspondence should be addressed. Telephone: (864) 656-5031. Fax: (864) 656-6613. E-mail: shwu@clemson.edu.

[†] Current address: Ferro Corporation, Washington, PA 15301.

(1) (a) Rowsell, J. L. C.; Yaghi, O. M. *Microporous Mesoporous Mater.* **2004**, *73*, 3–14, and references cited therein. (b) Férey, G. *Chem. Mater.* **2001**, *13*, 3084–3098.

(2) (a) Mitzi, D. B.; Wang, S.; Feild, C. A.; Chess, C. A.; Guloy, A. M. *Science* **1995**, *267*, 1473–1476. (b) Mitzi, D. B.; Field, C. A.; Harrison, W. T. A.; Guloy, A. M. *Nature* **1994**, *369*, 467–469, and references cited therein.

(3) For example, (a) Huang, X.; Li, J.; Zhang, Y.; Mascarenhas, A. *J. Am. Chem. Soc.* **2003**, *125*, 7049–7055. (b) Zheng, N.; Bu, X.; Feng, P. *Nature* **2003**, *426*, 428–432. (c) Zheng, N.; Bu, X.; Wang, B.; Feng, P. *Science* **2002**, *198*, 2366–2369. (d) Klimov, V. I.; Mikhailovsky, A. A.; Xu, S.; Malko, A.; Hollingsworth, J. A.; Leatherdale, C. A.; Eisler, H. J.; Bawendi, M. G. *Science* **2000**, *290*, 314–317.

(4) (a) Wang, S.; Hwu, S.-J. *J. Am. Chem. Soc.* **1995**, *117*, 5515–5522. (b) Wang, S.; Hwu, S.-J. *Inorg. Chem.* **1995**, *34*, 166–171. (c) Chen, S. C.; Ramanujachary, K. V.; Greenblatt, M. *Inorg. Chem.* **1994**, *33*, 5994–5998. (d) Wang, S.; Hwu, S.-J. *J. Am. Chem. Soc.* **1992**, *114*, 6922–6923.

10.1021/cm701995d CCC: $37.00 
Published on Web 11/13/2007

because of confined electrons.[5] Also, a couple of homologous chalcogenide series $AE_2M_{1+n}Q_{3+n}$ (AE = Sr and Ba; M = Sb and Sn; Q = S and Se; $n$ = integers $\geq 1$) has recently been reported, where the structure is built up from the stacking of 2D building units of the rock salt and fluorite types.[6] These last two all-inorganic compound families were isolated at rather high temperature, which suggests that the rational design in the thermodynamic systems is conceptually feasible based on the same bonding principles.

There are emerging activities in exploring hybrid solids with mixed ionic/covalent composite structure, and the new phase formation has continued to extend our knowledge in the structure and bonding of such a fascinating class of materials.[7] Some recent findings include salt-inclusion solids (SISs) in the transition-metal oxide[5e,8] as well as main-group oxide systems, where ionic salt (such as alkali metal halides) revealed template-like functions for the formation of metal oxide nanostructures.[9] These intriguing SISs resemble the MOF solids featuring zero- (clusters), one- (chains), and two- (sheets) dimensional, as well as porous metal-oxide structures. We have recently extended this study into the chalcogenide-based systems, where little salt inclusion chemistry is known. In light of the recent discovery of a new chalcohalide compound family, we have continued the systematic exploratory synthesis of mixed chalcogenide/halide chemical systems.[10] This paper reports the second chalcohalide series to further demonstrate the utilities of mixed-anion reactions in the formation hybrid framework solids.

These new discoveries have suggested that the introduction of halide anions allows for the formation of the dimensionally reduced metal chalcogenide framework. The resulting solids often contain nanostructures of metal chalcogenide adopting the coordination geometry and polyhedron connectivity of the corresponding bulk. The subsequent properties show a quantum confinement effect (QCE) similarly found in the inorganic/organic hybrid semiconductor as well as nanodots.[11]

Prior to the current study, some compound families involving post-transition-metal cations in question have been reported in the halide-containing ternary antimony/bismuth chalcohalide systems: MQX (M = Sb and Bi; Q = S, Se, and Te; X = halogen), $Bi_4Se_5Cl_2$, $Bi_{19}Se_{27}Cl_3$, $Bi_{11}Se_{12}Cl_9$, and $Bi_3Se_4Br$.[12] In our follow-up studies, we have completed the synthesis of the first chalcohalide series, $CdMQ_2X$ (M = Sb and Bi; Q = S and Se; X = Cl, Br, and I), reported in ref 10 with the exception of "$CdSbSe_2Br$".[13] It was observed that the compound formation is limited to the combination of chalcogenides ($Q^{2-}$) and halides ($X^-$), where X is from either the same row of the Periodic Table as Q or immediately below. Dependent upon the size of Q/X, there were two types of structures formed.

During the search for $CdSbSe_2Br$, we have isolated the title compound and, through cation substitutions, its In derivatives. In the present work, we report the results of solid-state synthesis, crystal structure, spectroscopy, and electronic band structures of this new quaternary chalcohalide compound $CdSb_2Se_3Br_2$ **1** (1232) and its In derivatives $InSb_2S_4Cl$ **2**, $InSb_2S_4Br$ **3**, $InSb_2Se_4Br$ **4**, and $InBi_2Se_4Br$ **5** (1241). This newly discovered chalcohalide family shows the quantum confinement effect of the optical band gap, which is the first example among inorganic mixed-anion compounds reported thus far.

## Experimental Section

**General Procedures.** All of the reactants were loaded in a nitrogen-filled dry box. The reaction mixtures were sealed in a fused quartz tube under vacuum ($\sim 10^{-4}$ torr) using a methane torch. The materials were examined using powder X-ray diffraction (PXRD) patterns recorded on a SCINTAG 2000 diffractometer equipped with a graphite monochromator (Cu K$\alpha_1$ radiation). Single-crystal

(5) (a) Queen, W.; Hwu, S.-J.; Wang, L. *Angew. Chem., Int. Ed.* **2007**, *46*, 5344–5347. (b) Ranmohotti, K. G. S.; Mo, X.; Smith, M. K.; Hwu, S.-J. *Inorg. Chem.* **2006**, *45*, 3665–3670. (c) Mo, X.; Etheredge, K. M. S.; Hwu, S.-J.; Huang, Q. *Inorg. Chem.* **2006**, *45*, 3478–3480. (d) Ulutagay-Kartin, M.; Hwu, S.-J.; Clayhold, J. A. *Inorg. Chem.* **2003**, *42*, 2405–2409. (e) Hwu, S.-J.; Ulutagay-Kartin, M.; Clayhold, J. A.; Mackay, R.; Wardojo, T. A.; O'Connor, C. T.; Krawiec, M. *J. Am. Chem. Soc.* **2002**, *124*, 12404–12405. (f) Clayhold, J. A.; Ulutagay-Kartin, M.; Hwu, S.-J.; Koo, H.-J.; Whangbo, M.-H.; Voigt, A.; Eaiprasertsak, K. *Phys. Rev. B: Condens. Matter Mater. Phys.* **2002**, *66*, 052403/1052403/4. (g) Ulutagay-Kartin, M.; Etheredge, K. M. S.; Schimek, G. L.; Hwu, S.-J. *J. Alloys Compd.* **2002**, *338*, 80–86. (h) Hwu, S.-J. *Chem. Mater.* **1998**, *10*, 2846–2859.

(6) (a) Kabbour, H.; Cario, L. *Inorg. Chem.* **2006**, *45*, 2713–2717. (b) Kabbour, H.; Cario, L.; Danot, M.; Meerschaut, A. *Inorg. Chem.* **2006**, *45*, 917–922. (c) Fluorite and rock salt examples: Cario, L.; Kabbour, H.; Meerschaut, A. *Chem. Mater.* **2005**, *17*, 234–236. (d) Kabbour, H.; Cario, L.; Boucher, F. *J. Mater. Chem.* **2005**, *15*, 3525–3531. (e) Cario, L.; Lafond, A.; Morvan, T.; Kabbour, H.; Deudon, C.; Andre, G.; Palvadeau, P. *Solid State Sci.* **2005**, *7*, 936–944.

(7) (a) Tulsky, E. G.; Long, J. R. *Chem. Mater.* **2001**, *13*, 1149–1166. (b) Tulsky, E. G.; Long, J. R *Inorg. Chem.* **2001**, *40*, 6990–7002.

(8) (a) Mo, X.; Ferguson, E.; Hwu, S.-J. *Inorg. Chem.* **2005**, *44*, 3121–3126. (b) Mo, X.; Hwu, S.-J. *Inorg. Chem.* **2003**, *42*, 3978–3980. (c) Huang, Q.; Ulutagay-Kartin, M.; Mo, X.; Hwu, S.-J. *Mater. Res. Soc. Symp. Proc.* **2003**, *755*, DD12.4.1. (d) Huang, Q.; Hwu, S.-J. *Inorg. Chem.* **2003**, *42*, 655–657. (e) Huang, Q.; Hwu, S.-J.; Mo, X. *Angew Chem., Int. Ed.* **2001**, *40*, 1690–1693. (f) Huang, Q.; Ulutagay, M.; Michener, E. A.; Hwu, S.-J. *J. Am. Chem. Soc.* **1999**, *121*, 10323–10326. (g) Ulutagay, M.; Schimek, G. L.; Hwu, S.-J.; Taye, H. *Inorg. Chem.* **1998**, *37*, 1507–1512.

(9) (a) $[Na_3F][SnSi_3O_9]$: Liao, C.-H.; Chang, P.-C.; Kao, H.-M.; Lii, K.-H. *Inorg. Chem.* **2005**, *44*, 9335–9339. (b) $NaSmGe_4Se_4 \cdot 0.25Na_2Se$: Choudhury, A.; Dorhout, P. K. *Inorg. Chem.* **2006**, *45*, 5245–5247. (c) $[Cd(C_2O_4)_6] \cdot KCl \cdot 2H_2O$: Vaidhyanathan, R.; Neeraj, S.; Prasad, P. A.; Natarajan, S.; Rao, C. N. R. *Angew. Chem., Int. Ed.* **2000**, *39*, 3470–3473. (d) $Cr_3Si_2O_7 \cdot 0.25NaCl$: Schmidt, A.; Glaum, R. *Inorg. Chem.* **1997**, *36*, 4883–4887.

(10) Wang, L.; Hung, Y.-C.; Hwu, S.-J.; Koo, H.-J.; Whangbo, M.-H. *Chem. Mater.* **2006**, *18*, 1219–1225.

(11) (a) Fu, H. X.; Li, J. *J. Chem. Phys.* **2004**, *120*, 6721–6725. (b) Huang, X. Y.; Li, J.; Zhang, Y.; Mascarenhas, A. *J. Am. Chem. Soc.* **2003**, *125*, 7049–7055. (c) Huang, X. Y.; Heulings, H. R., IV; Le, V.; Li, J. *Chem. Mater.* **2001**, *13*, 3754–3759. (d) Heulings, H. R., IV; Huang, X. Y.; Li, J. *Nano Lett.* **2001**, *1*, 521–525. (e) Huang, X. Y.; Li, J. *J. Am. Chem. Soc.* **2000**, *122*, 8789–8790. (f) Alivisators, A. P. *J. Phys. Chem.* **1996**, *100*, 13226–13239. (g) Hagfeldt, A.; Gratzel, M. *Chem. Rev.* **1995**, *95*, 49–68. (h) Fendler, J. H.; Meldrum, F. C. *Adv. Mater.* **1995**, *7*, 607–632. (i) Weller, H. *Adv. Mater.* **1993**, *5*, 88–95. (j) Steigerwald, M. L.; Brus, L. E. *Acc. Chem. Res.* **1990**, *23*, 183–188. (k) Henglein, A. *Chem. Rev.* **1989**, *89*, 1861–1873.

(12) (a) SbQX (Q = S, Se, and Te; X = halogen): Ibanez, A.; Jumas, J. C.; Olivier-Fourcade, J.; Philippot, E.; Maurin, M. *J. Solid State Chem.* **1983**, *48*, 272–283. (b) BiQX (Q = S, Se, and Te; X = halogen): Oppermann, H.; Petasch, U. *Z. Naturfursch., B: Chem. Sci.* **2003**, *58*, 725–740. (c) $Bi_4Se_5Cl_2$: Krämer, V. *Z. Naturfursch., B: Chem. Sci.* **1976**, *31*, 1542–1543. (d) $Bi_{19}Se_{27}Cl_3$: Krämer, V. *Z. Naturfursch., B: Chem. Sci.* **1974**, *29*, 688–689. (e) $Bi_{11}Se_{12}Cl_9$: Eggenweiler, U.; Keller, E.; Krämer, V.; Petasch, U.; Oppermann, H. *Z. Kristallogr.* **1999**, *214*, 264–270. (f) $Bi_3Se_4Br$: Petasch, U.; Söhnel, T.; Oppermann, H.; Eggenweiler, U.; Keller, E.; Krämer, V. *Z. Naturfursch., B: Chem. Sci.* **2000**, *55*, 273–276.

(13) Wang, L., Ph.D. Dissertation, May 2007.

X-ray structure analysis was carried out on a Rigaku AFC-8S four-circle diffractometer (Mo Kα = 0.710 73 Å) equipped with the Mercury charge coupled device (CCD) area detector. Semiquantitative chemical analysis of single crystals was performed by energy-dispersive X-ray (EDX) analysis using a Hitachi S-3500 scanning electron microscope equipped with an OXFORD EDX microprobe.

**Synthesis.** Compound **1** was initially obtained as a byproduct from the reaction in an attempt to isolate single crystals of the "$CdSbSe_2Br$" phase using a slight excess amount of low-melting elemental selenium (mp = 217 °C). The as-purchased CdSe (Mallinckrodt, 98%), $CdBr_3$ (Aldrich, 99.9%), antimony (Aldrich, 99.99%), and selenium (Aldrich, 99.99%) were loaded according to the molar ratio of 1:1:2:4. The reaction mixture was sealed under vacuum in a carbon-coated quartz ampule and heated to 500 °C at a rate of 1 °C/min. It was then isothermed for 3 days, followed by slow cooling at a rate of 3 °C/h to room temperature. Black, needle-shaped crystals of $CdSb_2Se_3Br_2$ were isolated in a low yield (<5%) from the reaction products, which were primarily CdSe (50%), $Sb_2Se_3$, and SbSeBr. The final composition of the compound was determined first by the X-ray single-crystal structure analysis and EDX and then via successful stoichiometric synthesis.

**Stoichiometric Synthesis.** After the structural identification, the stoichiometric syntheses of the polycrystalline selenobromide compound were carried out using reaction mixtures as shown in eqs 1 and 2

$$CdBr_2 + 2Sb + 3Se \rightarrow CdSb_2Se_3Br_2 \quad (1)$$

$$CdBr_2 + Sb_2Se_3 \rightarrow CdSb_2Se_3Br_2 \quad (2)$$

The reactants used, including their sources and purities, are as follows: $CdBr_2$ (Strem, 99.9+% Cd), Sb (Alfa Aesar, 99.5%), Se (Aldrich, 99.99%), and $Sb_2Se_3$ (Alfa Aesar, 99.999%). The reactions were heated directly to 450 °C (1 °C/min) and isothermed for 4 days followed by slow cooling to room temperature. Attempts to isolate other members of the $CdM_2Q_3X_2$ chalcohalide family (X = Cl, Br, and I; M = Sb and Bi) and selected transition-metal-containing analogues, such as "$HgBi_2Se_3Br_2$" and "$MnBi_2Se_3Br_2$" all failed. Instead, binary phases $Sb_2Q_3$ and $Bi_2Q_3$ along with ternary phases SbSeI and SbSX (X = Br and I)[12a] as well as previously reported $CdMQ_2X$ were obtained.[10] This suggests that the $CdSb_2Se_3Br_2$ phase can only be formed possibly in a narrow phase region in the $CdBr_2$/Sb/Se phase diagram. It also means that, although this phase is thermodynamically stable, the window of conditions to formulate this phase is narrow.

Four indium-substituted phases, **2**–**5**, were isolated, and single crystals were obtained from direct interaction of stoichiometric mixtures as outlined in eq 3 at 450 °C

$$3In + MX_3 + 5M + 12Q \rightarrow 3InM_2Q_4X \quad (3)$$

where M/Q/X = Sb/S/Cl **2**, Sb/S/Br **3**, Sb/Se/Br **4**, and Bi/Se/Br **5**, respectively. Crystals of **2**–**5** had dark brown and amber colors, which indicate that the compounds are likely semiconductors at best.

Out of eight possible combinations in the In/M/Q/X series, two indium bismuth sulfohalides $InBi_2S_4X$ (X = Cl and Br) were reported prior to this study.[14] These known phases were first synthesized via vapor transport reactions, employing $S_2Cl_2$ as transporting agents or incorporation of bromine element, and then reproduced by using the solid-state reactions in this study. As shown in Figure 1, the **2**–**5** phases form a different structure than $InBi_2S_4X$ (see later discussion). We thus denote the previously discovered 1241 structure type I and the current one type II.

Furthermore, the Sb- and Bi-containing 1241 selenoiodide phases failed to form. The PXRD patterns of the products from stoichiometric reactions show evidence of the formation of a new phase (see Figure S1a in the Supporting Information. The indium bismuth selenoiodide was later identified as $In_2Bi_3Se_7I$ by single-crystal X-ray diffraction (SXRD) methods.[13,15] Attempts to prepare the Sb-1241 and Sb-2371 phases resulted in a stoichiometric amount of SbSeI and $InSbSe_3$. It should also be noted that the combinations of S/I or Se/Cl have always failed to form quaternary compounds, possibly because of the size mismatch of anions also observed in the 1121 series.[10]

**X-ray Structure Analysis.** The needle-shape single crystals were mounted on the quartz fiber for the SXRD data collection at room temperature. The structures were solved with direct methods and refined on $F^2$ with the full-matrix, least-squares method by SHELXL-97 of the SHELXTL program suite.[16] Each final refinement included anisotropic displacement parameters and a secondary extinction correction. Additional experimental details and crystallographic data are listed in Table 1. The atomic coordinates and selected bond distances and angles of $CdSb_2Se_3Br_2$ and a representative compound $InSb_2Se_4Br$ are in Tables 2 and Tables S2 and S3 in the Supporting Information, respectively. PXRD patterns of all of the stoichiometrically synthesized products were employed to confirm the formation of the bulk samples.

**Differential Thermal Analysis (DTA).** DTA was performed with a computer-controlled TA DTA-2000 thermal analyzer (TA Instruments, New Castle, DE). (see Figure S2 in the Supporting Information) The powder sample of ground single crystals (~10 mg) was sealed in quartz ampoules under a vacuum. A quartz ampoule containing alumina of equal mass was sealed and placed on the reference side of the detector. The samples were heated to 800 °C at 10 °C/min and isothermed for 5 min, followed by cooling at 10 °C/min to room temperature, and this heating/cooling cycle was repeated twice on the same sample. After each experiment, the samples were examined by PXRD, while single crystals, when available, were employed to determine unit-cell parameters by SXRD for phase identification.

**Diffuse Reflectance UV–Vis Spectrum.** Diffuse reflectance UV–vis spectra were recorded on a Shimadzu 3901 spectrophotometer accessorized with an integrating sphere. The polycrystalline samples were ground and smeared on the surface of the $BaSO_4$ sample holder prior to the measurement. The absorption data ($\alpha/S$) in the range of ~0.5–6.5 eV (190–2400 nm) were calculated from the reflectance mode using the Kubelka–Munk function $\alpha/S = (1 - R)^2/2R$, where $R$ is the reflectance at a given energy, $\alpha$ is the absorption, and $S$ is the scattering coefficient.[17] The energy gap was determined as the intersection point between the energy axis at the absorption offset and the line extrapolated from the linear portion of the absorption edge in the $\alpha/S$ versus energy (eV) plot.

(14) Krämer, V. *Mater. Res. Bull.* **1976**, *11*, 183–188.

(15) New compound $In_2Bi_3Se_7I$ was isolated from the In/Bi/Se/I reaction. It crystallizes in an orthorhombic crystallographic system with space group *Pnma* (number 62): $a$ = 26.623(5) Å, $b$ = 4.1380(8) Å, $c$ = 13.542(3) Å, $V$ = 1491.9(5) Å$^3$, and $Z$ = 4.

(16) Sheldrick, G. M. SHELXTL DOS/Windows/NT Version 6.12; Bruker Analytical X-ray Instruments, Inc.: Madison, WI, 2000.

(17) (a) Wendlandt, W. W.; Hecht, H. G. *Reflectance Spectroscopy*; Interscience: New York, 1966. (b) Kortüm, G. *Reflectance Spectroscopy*; Springer-Verlag: New York, 1969. (c) Kortüm, G.; Braun, W.; Herzog, G. *Angew. Chem., Int. Ed.* **1963**, *2*, 333–404.

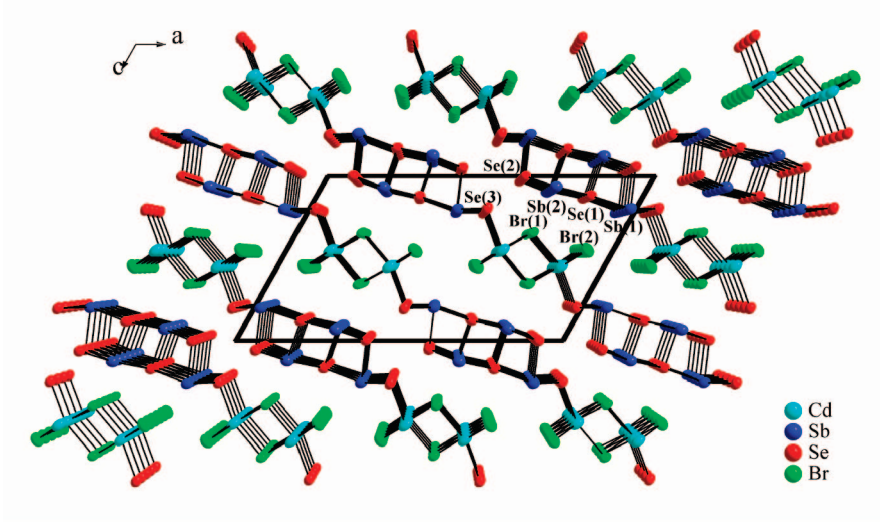


(a)

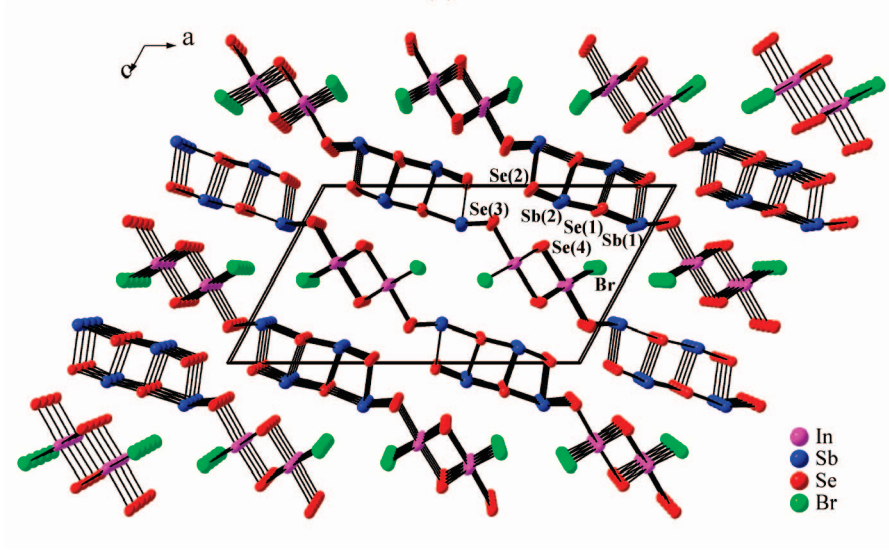


(b)

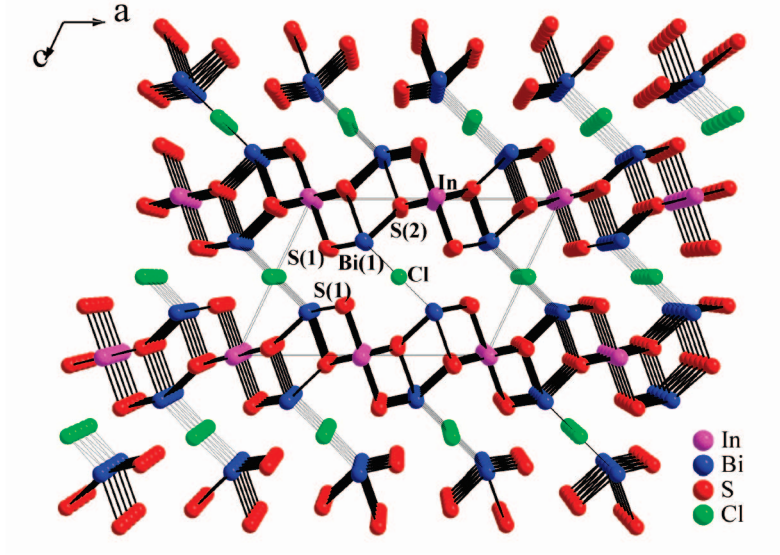


(c)

**Figure 1.** Perspective views of the structures of (a) $CdSb_2Se_3Br_2$, (b) $InSb_2Se_4Br$, and for comparison, (c) $InBi_2S_4Cl$ (with the long Bi–S bond being omitted for clarity).

**Table 1. Crystallographic Data for $CdSb_2Se_3Br_2$ and $InM_2Q_4X$**

| | 1 | 2 | 3 | 4 | 5 |
|---|---|---|---|---|---|
| empirical formula | $CdSb_2Se_3Br_2$ | In $Sb_2S_4Cl$ | $InSb_2S_4Br$ | $InSb_2Se_4Br$ | $InBi_2Se_4Br$ |
| formula weight (amu) | 501.73 | 522.04 | 566.47 | 754.04 | 928.52 |
| crystal color, shape | black, needle | amber, needle | red, needle | black, needle | black, needle |
| crystal dimensions (mm) | 0.02 × 0.02 × 0.36 | 0.02 × 0.02 × 0.31 | 0.01 × 0.01 × 0.29 | 0.02 × 0.02 × 0.22 | 0.024 × 0.048 × 0.38 |
| crystal system | | | monoclinic | | |
| space group | | | *C*2/*m* (No. 12) | | |
| *a* (Å) | 20.998(4) | 19.877(3) | 20.177(4) | 20.772(5) | 20.832(3) |
| *b* (Å) | 4.0260(8) | 3.8520(7) | 3.8670(3) | 4.0020(8) | 4.1140(5) |
| *c* (Å) | 12.149(2) | 11.484(2) | 11.660(2) | 11.939(2) | 11.958(3) |
| $\beta$ (deg) | 119.00(3) | 117.75(2) | 119.13(4) | 118.14(3) | 118.15(3) |
| *V* (Å$^3$) | 898.3(3) | 778.2(4) | 795(3) | 875.2(3) | 903.6(4) |
| *Z* | 4 | 4 | 4 | 4 | 4 |
| *R*1/*wR*2 (all data) | 0.0623/0.0631 | 0.0287/0.0551 | 0.0480/0.0989 | 0.0291/0.0588 | 0.0263/0.0604 |
| GOF | 1.135 | 1.153 | 1.196 | 1.012 | 1.113 |
| $\Delta\rho_{min}/\Delta\rho_{max}$e (Å$^{-3}$) | 0.677/–0.789 | 0.0792/–1.152 | 2.718/–2.410 | 3.111/–1.249 | 2.14/–1.77 |

**Table 2. Atomic Coordinates and Equivalent Isotropic Displacement Parameters (Å$^2$) of $CdSb_2Se_3Br_2$ and $InSb_2Se_4Br$**

| atom | *x* | *y* | *z* | $U_{eq}$ (Å$^2$)[a] |
|---|---|---|---|---|
| | | $CdSb_2Se_3Br_2$ | | |
| Cd | 0.840 40(7) | 1/2 | 0.5468(1) | 0.0284(4) |
| Sb(1) | 0.045 15(6) | 0 | 0.7827(1) | 0.0209(3) |
| Sb(2) | 0.203 57(6) | 1/2 | 0.0901(1) | 0.0229(3) |
| Se(1) | 0.320 98(8) | 0 | 0.1384(2) | 0.0189(4) |
| Se(2) | 0.098 83(8) | 0 | 0.0253(2) | 0.0183(4) |
| Se(3) | 0.959 91(8) | 1/2 | 0.7843(2) | 0.0203(4) |
| Br(1) | 0.712 49(9) | 1/2 | 0.3508(2) | 0.0230(4) |
| Br(2) | 0.8959(1) | 0 | 0.4536(2) | 0.0317(5) |
| | | $InSb_2Se_4Br$ | | |
| In | 0.837 26(8) | 1/2 | 0.5600(2) | 0.0215(4) |
| Sb(1) | 0.047 08(8) | 0 | 0.7774(2) | 0.0208(4) |
| Sb(2) | 0.297 68(8) | 0 | 0.9080(2) | 0.0213(4) |
| Se(1) | 0.7120(1) | 1/2 | 0.3446(2) | 0.0181(5) |
| Se(2) | 0.1798(1) | 1/2 | 0.8590(2) | 0.0176(5) |
| Se(3) | 0.9616(1) | 1/2 | 0.7853(2) | 0.0185(5) |
| Se(4) | 0.0972(1) | 0 | 0.0229(2) | 0.0162(5) |
| Br | 0.8957(2) | 0 | 0.4654(2) | 0.0354(6) |

[a] Equivalent isotropic *U* defined as one-third of the trace of the orthogonalized $U_{ij}$ tensor.

**Electronic Band Structure Calculations.** The extended Hückel tight-binding (EHTB) electronic band structure calculations[18] were carried out for the overall lattice of **1**, as well as for the bromide-containing sublattice $[Cd_2SeBr_4]^{2-}{}_\infty$ and the antimony selenide sublattice $[Sb_4Se_5]^{2+}{}_\infty$, using the CASEAR program.[19] For a comparison, we also did the EHTB calculation on the binary $Sb_2Se_3$ phase (Figure S3 in the Supporting Information). The atomic orbital parameters employed in our calculations were listed in Table S1 in the Supporting Information.

## Results and Discussion

**Synthesis.** It is rather surprising to see that the $CdSb_2Se_3Br_2$ phase is the only compound that can be isolated thus far among the 12 possible phases in the $CdM_2Q_3X_2$ (1232) chemical system (where M = Sb and Bi; Q = S and Se; X = Cl, Br, and I). Via stoichiometric synthesis to isolate eight of these phases in the $CdM_2S_3X_2$ (X = Cl and Br) and $CdM_2Se_3X_2$ (X = Br and I) systems, we have observed the formation of the reported $CdMQ_2X$ (1121) phases instead with the exception of $CdSb_2Se_3Br_2$. The byproducts of these reactions were approximately equal amounts of MQX along with few crystals of $M_2Q_3$. Incidentally, the 1121 phase does not exist in the Cd–Sb–Se–Br system; instead, the title compound **1** was formed.

We have not yet been able to synthesize the four hypothetical $CdM_2S_3I_2$ and $CdM_2Se_3Cl_2$ phases (M = Sb and Bi) either, which could be attributed to the mismatch of the size of anions, S/I and Se/Cl, respectively. This was first realized in the formation of 1121 series,[10,13] where the 1121 chalcohalide phases could form only if the halide in question is from either the same row as the chalcogenide or the row immediately below. Furthermore, through matching the chalcogenide with different halide anions, one can control the formation of different structure types. If this were the general trend seen in chalcohalide compounds, it would explain why we have not seen the formation of the 1232 phase in these four mixed chalcohalide systems.

It is evident that the mixing of halide anions with chalcogenides, because of their different bonding nature, has played a fascinating role in the formation of special frameworks of antimony and bismuth chalcogenides. In the structure of the previously reported $CdSbS_2Cl$ phase, the $[Sb_2S_3]_\infty$ quasi-one-dimensional chains are formed upon the introduction of chloride anions. Seemingly, chloride serves as the structure "terminator" to cease the propagation of the metal–chalcogenide covalent networks. The same is true in this new family of chalcohalides, where the QCE has been observed in optical band gaps (see latter discussion).

Last, the DTA results show $CdSb_2Se_3Br_2$ and $InSb_2Se_4Br$ melt congruently at 509 and 466 °C, respectively. This means that the crystal growth can be achieved by employing own melt. The known 1241-I $InBi_2S_4Cl$ phase has reportedly shown an incongruent melting behavior (mp = 620 °C), and there were no evidence of solid-phase transition between the room temperature and the melting temperature.[14] Nevertheless, crystal growth has been achieved using a high-temperature, solid-state reaction in this study.

**Crystal Structures. 1** exhibits a new structure type closely related to that of $Bi_3Se_4Br$. The latter is one of the two observed selenohalide phases (see the list below) in the pseudo-binary $Bi_2Se_3$–$BiX_3$ systems.[12b] The four $InM_2Q_4X$ phases are isoelectronic and isostructural with **1**.

*$CdSb_2Se_3Br_2$.* The extended structure can alternatively be viewed as the result of an "insertion" of the $CdBr_2$ lattice

(18) (a) Whangbo, M.-H.; Hoffmann, R. *J. Am. Chem. Soc.* **1978**, *100*, 6093–6098. (b) Ammeter, J.; Bürgi, H.-B.; Thibeault, J.; Hoffmann, R. *J. Am. Chem. Soc.* **1978**, *100*, 3686.

(19) The calculations were carried out by employing the CAESAR2 program package (Dai, D.; Ren, J.; Liang, W.; Whangbo, M.-H. http://chvamw.chem.ncsu.edu/, 2002).

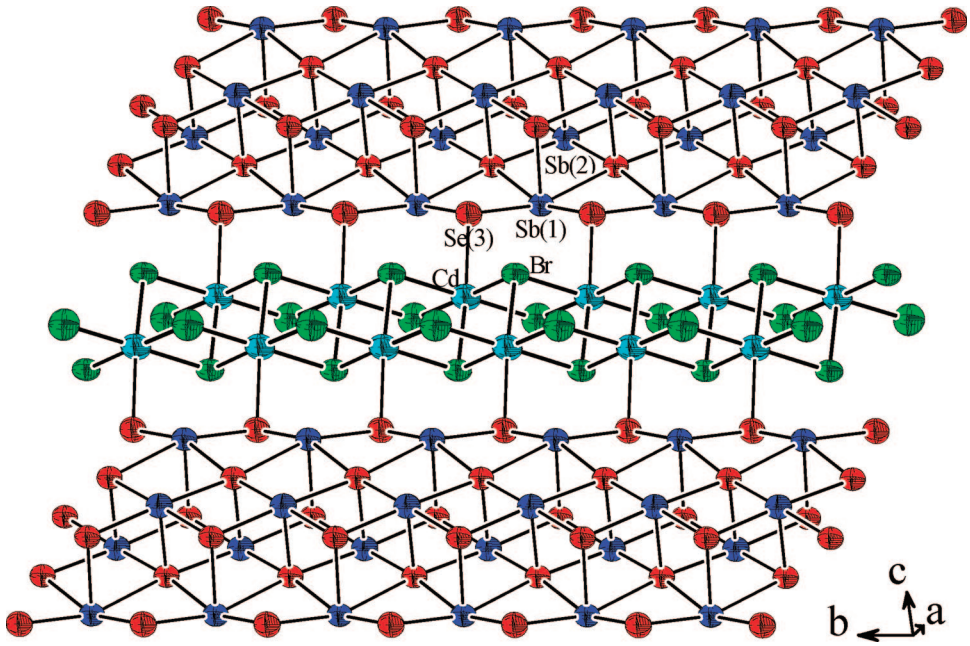


**Figure 2.** Connectivity of the structural units in **1**. Thermal ellipsoids are drawn at a 95% probability.

into the $Sb_2Se_3$ covalent framework. These two building units are linked through the Sb–Se–Cd bonds in an alternating fashion to form the composite $(CdBr_2)(Sb_2Se_3)$ slabs, which propagate along the (−101) plane (see Figure 1a). The parallel slabs are stacked along the [–101] direction, and the neighboring slabs are displaced by a building unit. This results in the closest interslab distance of 3.481(5) Å through the Se(1)–Br interaction. Meanwhile, the lone-pair electrons of the $Sb_2Se_3$ unit are pointing into the interslab space giving rise to the closest Sb(1)–Br distance of 3.695(9) Å. That means that the interslab interaction is primarily electrostatic. This is consistent with the morphology of the needle crystals that are made of bundles and can easily be split apart.

Figure 2 shows that the $CdBr_2$ and $Sb_2Se_3$ structural units adopt the (110) and (100) NaCl structure, respectively. The structure formulas of each extended sublattices can be expressed as $[Cd_{2/1}Br_{2(2/3)}Br_{2(1/3)}Br_{4/2}Se_{2/2}]^{2-}{}_\infty$ ($\equiv[Cd_2Br_4Se]^{2-}{}_\infty$) and $[Sb_{4/1}Se_{2(2/3)}Se_{2(3/5)}Se_{4(1/4)}Se_{2(1/3)}Se_{2(2/5)}]^{2+}{}_\infty$ ($\equiv[Sb_4Se_5]^{2+}{}_\infty$), respectively. The former consists of dual octahedral chains of Cd-centered $[CdBr_5Se]$ units sharing *cis* Br edges, and the chains propagate along the *b* axis via sharing *trans* Br edges of the octahedra. The second sublattice adopts a common structural unit seen in antimony-containing selenides. It is formed via edge-shared $SbSe_5$ square pyramids with lone-pair electrons of the $Sb^{3+}$ cations pointing into the interslab space.

*$InM_2Q_4X$.* Phases **2**–**5** are isostructural, and for simplicity, only the structure of $InSb_2Se_4Br$ **4** is discussed (see Figure 1b). For a comparison, the structure of the isomorphous $InBi_2S_4Cl$[14] phase is shown in Figure 1c.

The structure of **4** can be related to that of **1** by the isoelectronic substitution of InSeBr for the $CdBr_2$ subunit, and the structure formula can thus be written as $(InSeBr)(Sb_2Se_3)$. In the structure refinement, the additional Se that substitutes for one of the Br sites could be assigned arbitrarily because of the indistinguishable electron count between these two anions. Consecutive structure refinements of $InSb_2S_4Br$ **3** helped determine the final positions of anions. The resulting structure has all of the metal cations interconnected through chalcogenide anions, with the halide anions pointing into the interslab space (Figure 1b). As seen in $CdSb_2Se_4Br$, the $[In_2Q_3X_2]^{2-}{}_\infty$ and $[Sb_4Se_5]^{2+}{}_\infty$ sublattices are interlinked by a selenide anion, Se(3), to form hybrid slabs.

The structure (type I) of $InBi_2S_4X$ (X = Cl and Br), on the other hand, is made of parallel $[InBi_2S_4]^{+}{}_\infty$ slabs interlinked by $Cl^-/Br^-$ anions, as shown in Figure 1c. As discussed earlier, the structure of these isomorphous phases is designated as 1241-I and that of **2**–**5** as 1241-II. Meanwhile, the formation of these two structure types has little to do with the reaction conditions as evidenced by the fact that the crystals of $InBi_2S_4Cl$ (1241-I) can be grown by employing either chemical vapor transport or solid-state methods. It is interesting that the 1241-I structure is only found in the $InBi_2S_4X$ (X = Cl and Br) family.

**Structural Comparison with $Bi_3Se_4Br$.** The projected views reveal similar structure features between **1** and previously discovered $Bi_3Se_4Br$ (Figure 3a). The latter can in fact be written as $[BiSeBr][Bi_2Se_3]$, and it can also be written with the general formula of the 1241 structure, $BiBi_2Se_4Br$. While the $[Bi_2Se_3]$ sublattice matches exactly with those of the corresponding $M_2Q_3$ sublattice in 1232, 1241-I, and 1241-II, the [BiSeBr] structural unit is different because of varied coordination geometry around Bi. Figure 3b shows the local geometry of the metal cations with respect to the halide ($Br^-$) anions, e.g., $BiSe_3Br_4$ (left) in the reported structure of $Bi_3Se_4Br$, $CdSeBr_5$ (center) in 1232, and $InSe_4Br_2$ (right) in the 1241 structure. It is clear that the trivalent $Bi^{3+}$ cation adopts an additional coordination compared to $In^{3+}$, while the overall charge of the $[BiSe_3Br_4]^{7-}$ polyhedral unit remains the same as that of $[InSe_4Br_2]^{7-}$. Figure 3c shows the connectivity of the bromide-containing $[Bi_2Se_4Br_2]^{4-}{}_\infty$ sublattice propagating along [010], in which the neighboring rows of $Bi^{3+}$ cations are head-to-head as opposed to side-

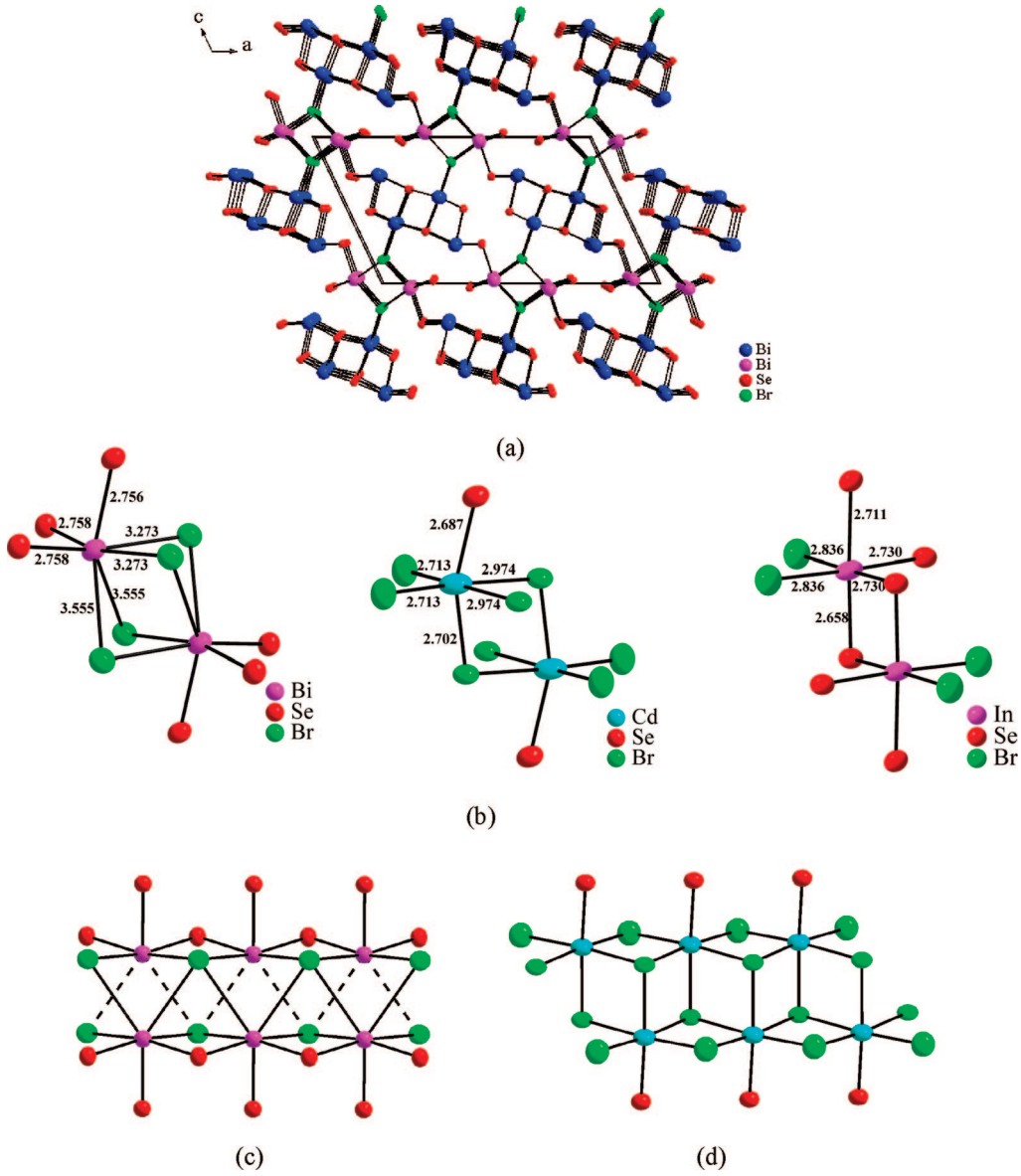


**Figure 3.** (a) Perspective view of $Bi_3Se_4Br$, (b) local coordination of cations in $Bi_3Se_4Br$ (left), $CdSb_2Se_3Br_2$ (center), and $InSb_2Se_4Br$ (right), and (c and d) partial structure of the fused $[BiSe_3Br_4]^{7-}$ polyhedral and $[CdBr_2]$ octahedral chains. Selected bond distances are included in b for a comparison (see the text). For identification, the Bi atoms residing in different sublattices are labeled in different colors accordingly. Thermal ellipsoid are drawn at a 95% probability.

by-side, such as $Cd^{2+}$ in Figure 3d, to accommodate the variation in the coordination geometry of Bi. The results of BVS analysis for the three polyhedra are listed in Table 3, confirming the formal charges of $Bi^{3+}$ as well as $Cd^{2+}$ and $In^{3+}$.

The $[BiSe_3Br_4]$ and $[CdSeBr_5]$ polyhedral units are much more distorted than $[InSe_4Br_2]$ (see Figure 3b). One would expect to see an elongation of bromide bonds to accommodate the Columbic repulsion between two highly charged trivalent cation centers through the shared edge. This distortion could be predominately due to the lone-pair electrons in the valence shell of the $Bi^{3+}$ cations. In the absence of lone-pair electrons in $In^{3+}$, the In-centered polyhedra are thus only slightly distorted.

In light of the rich chemistry in the pseudo-binary $Bi_2Se_3$–$BiCl_3$ system, we also explored the pseudo-binary phase diagram of $CdBr_2$–$Sb_2Se_3$ along the $(CdBr_2)_n(Sb_2Se_3)_m$ ($n$ and $m$ are positive integers) phase line. It is worth noting

**Table 3. BVS Values for the Cd-, In-, and Bi-Containing Compounds**

| | Bi | BVS |
|---|---|---|
| Se(3) | 0.841 | 2.23 |
| Se(4) | 0.837 × 2 | 2.09 |
| Br | 0.180 × 2 + 0.084 × 2 | 0.90 |
| BVS | 3.04 | |

| | Cd | BVS |
|---|---|---|
| Se(3) | 0.480 | 1.97 |
| Br(1) | 0.191 × 2 + 0.399 | 2.09 |
| Br(2) | 0.387 × 2 | 0.87 |
| BVS | 2.04 | |

| | In | BVS |
|---|---|---|
| Se(1) | 0.506 × 2 + 0.615 | 1.93 |
| Se(3) | 0.532 | 2.02 |
| Br | 0.329 × 2 | 0.92 |
| BVS | 2.82 | |

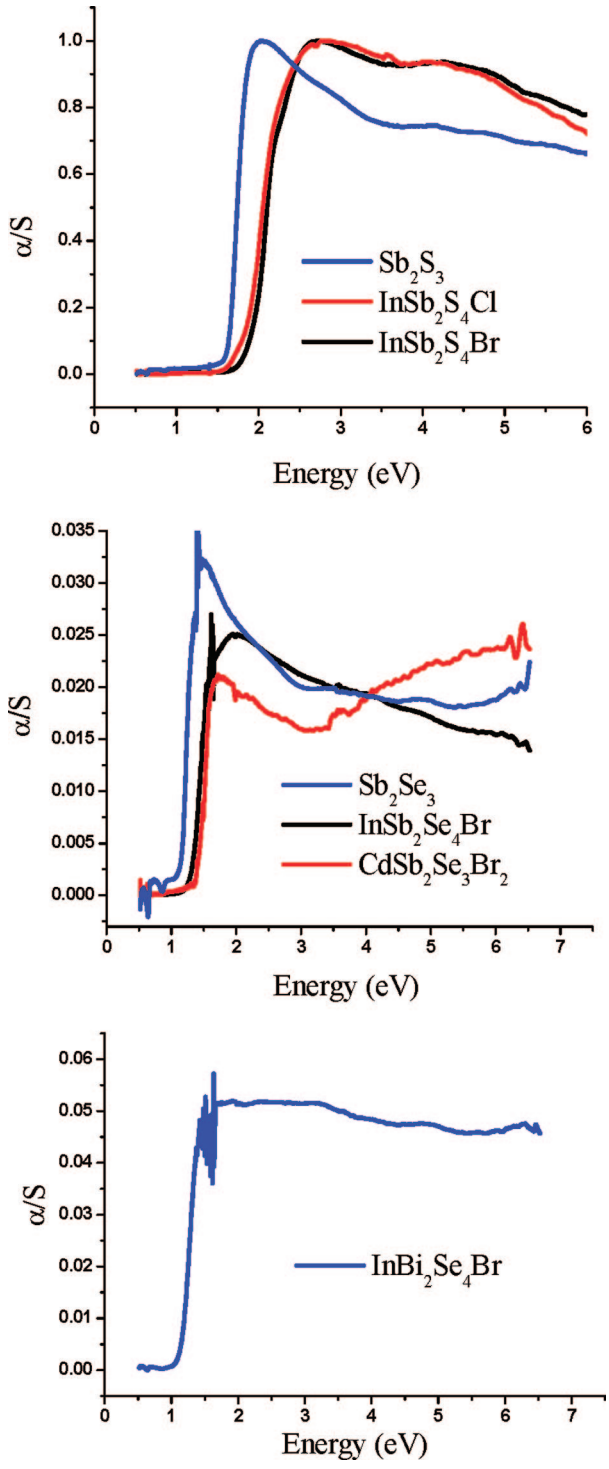


**Figure 4.** UV–vis spectra of the title compounds along with the binary $Sb_2S_3$ and $Sb_2Se_3$ for a comparison. The spectrum of narrow band gap $Bi_2Se_3$ ($E_g$ = 0.3 eV) is not available because of instrument limitation. A blue shift is evident for the title compounds containing nanostructured $M_2Q_3$ sublattices (see the text).

that there are five existing $Bi_2Se_3$–$BiCl_3$ phases with relative ratios quoted in parenthesis: $Bi_{19}Se_{27}Br_3$ (9:1), $Bi_3Se_4Br$ (4:1), $Bi_4Se_5Cl_2$ (5:2), $Bi_{11}Se_{12}Cl_9$ (4:3), and BiSeCl (1:2). The first two $Bi_2Se_3$-rich phases form mixed frameworks that contain the $[Bi_2Se_3]$ building blocks. For the last three, the structure consists of "folded ladders" related to that in the BiSeCl structure.[12b,c,e] In any event, we have yet been able to produce additional phases other than $CdSb_2Se_3Br_2$ ($n/m$ = 1:1).

**Table 4. Observed Optical Band Gap Energies[a] for the Title Compounds along with Binary Phases for a Comparison**

| compounds | $E_g$ (eV) | compounds | $E_g$ (eV) |
|---|---|---|---|
| $Sb_2S_3$ | 1.60 | | |
| $InSb_2S_4Cl$ (**2**) | 1.80 | $InSb_2S_4Br$ (**3**) | 1.80 |
| $Sb_2Se_3$ | 1.11 | | |
| $CdSb_2Se_3Br_2$ (**1**) | 1.40 | $InSb_2Se_4Br$ (**4**) | 1.35 |
| $Bi_2S_3$ | 1.30 | | |
| $InBi_2S_4Cl$[b] | 1.50 | $InBi_2S_4Br$[b] | 1.50 |
| $Bi_2Se_3$ | 0.30 | | |
| $InBi_2Se_4Br$ (**5**) | 1.21 | $In_2Bi_3Se_7I$[c] | 1.38 |

[a] The reported band gap energies for $Sb_2S_3$ and $Sb_2Se_3$ are 1.95–2.20 and 1.11 eV, respectively, and the reported band gap energies for $Bi_2S_3$ and $Bi_2Se_3$ are 1.30 and 0.30 eV, respectively. The UV–vis spectra have also been recorded for a comparison. [b] Compounds that adopt the 1241-I structure were synthesized by conventional solid-state reactions (see the text). [c] New compound $In_2Bi_3Se_7I$ (see ref 15).

**UV–Vis Spectra and Electronic Band Structure Calculations.** The reflectance spectra of **1–5** along with those of $Sb_2Q_3$ (Q = S and Se) are shown in Figure 4. The UV–vis reflectance spectroscopy and band structure calculations prove that these compounds are semiconductors with steep band gap absorption edges around 1.1–1.8 eV. According to the crystal structures of the title compounds, the sublattices are likely electronically confined; in turn, the optical band gaps are expected to be widened because of the reduced dimensionality of respective chalcogenide sublattices. The band gaps of the title series together with those of $Sb_2S_3$, $Sb_2Se_3$,[20] $Bi_2S_3$, and $Bi_2Se_3$[21] are summarized in Table 4. Consequently, the increments of optical band gaps have been around 0.2–0.3 eV for all of the observed phases, except for $InBi_2Se_4X$ (0.9–1.0 eV), intuitively because of the quantum confinement effect (see the discussion below).

As shown in Figure 4, the absorption edges of all of the phases are sharp and show noticeable blue shifts compared to those of the corresponding binary $M_2Q_3$ chalcogenide phases. The optical band gap energies of these phases are seemingly independent of the halogen-incorporated sublattices but dictated by the dimensionally reduced $M_2Q_3$ component. The theoretical band structure calculations presented below offer some qualitative analysis to account for the origin of the observed blue shift.

**Electronic Band Structure.** The total density-of-states (DOS) derived from the extended Hückel tight binding (EHTB) electronic band structure calculations of **1** is presented in Figure 5a, and the partial DOS of $[Cd_2Br_4Se]^{2-}{}_\infty$ and $[Sb_4Se_5]^{2+}{}_\infty$ units are shown in parts b and c of Figure 5, respectively. The calculations have also been done for the other members of the title series. The results are fairly compatible with each other; we, therefore, are making our discussion based on the calculations for $CdSb_2Se_3Br_2$ hereafter. The calculated band structures for $Sb_2Se_3$ are included in Figure S3 in the Supporting Information for a comparison.

The calculated band structures are in a good agreement with the experimental results listed in Table 4, suggesting that both $CdSb_2Se_3Br_2$ and $Sb_2Se_3$ are semiconductors. For

(20) (a) Fujita, T.; Kurita, K.; Tokiyama, K; Oda, T. *J. Phys. Soc. Jpn.* **1987**, *56*, 3734–3739. (b) Wood, C.; Shaffer, J. C.; Proctor, W. G. *Phys. Rev. Lett.* **1972**, *29*, 485–487.
(21) Black, J.; Conwell, E. M.; Seigle, L.; Spencer, C. W. *J. Phys. Chem. Solids* **1957**, *2*, 240–251.

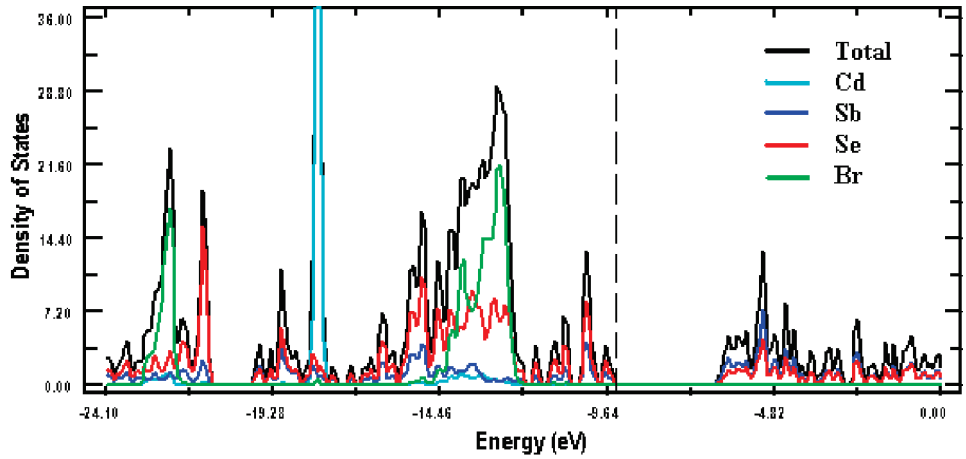


(a)

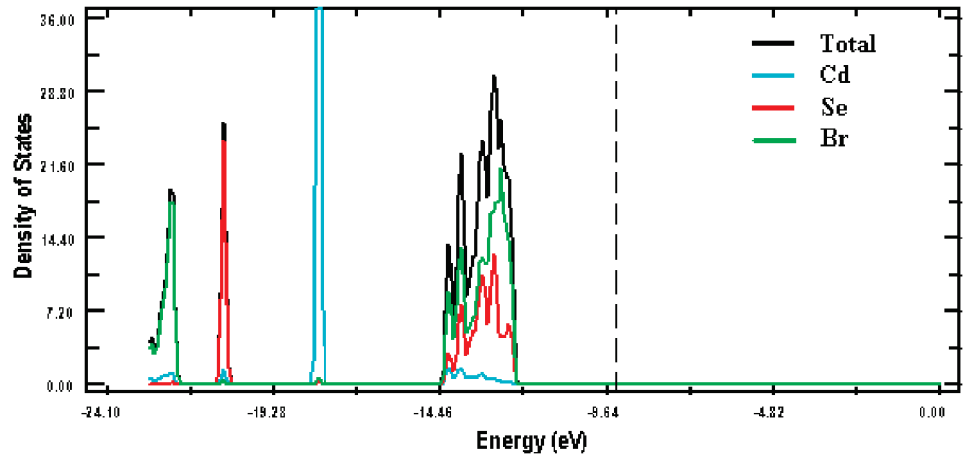


(b)

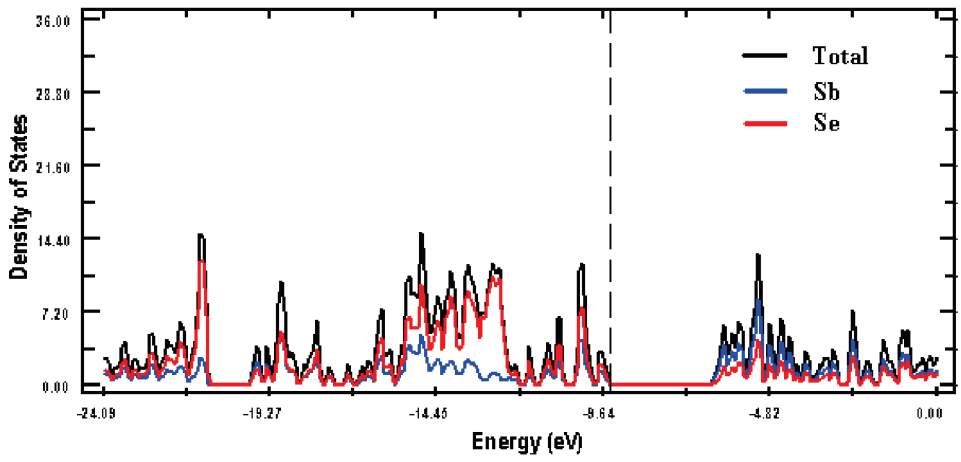


(c)

**Figure 5.** Plots of the total and partial DOS calculated for (a) $CdSb_2Se_2Br$ and two sublattices (b) $[Cd_2Br_4Se]^{2-}{}_\infty$ and (c) $[Sb_4Se_5]^{2+}{}_\infty$. The dashed line indicates the position of the Fermi level.

each $[CdSb_2Se_3Br_2]$ slab, the valence band top (VBT) is formed by the Sb–Se bonding orbitals (5s of Sb and 4p of Se) and the conduction band bottom (CBB) by the Sb–Se antibonding levels (Figure 5a). For the $[Sb_4Se_5]^{2+}{}_\infty$ sublattice, it can physically be considered nanostructures of $Sb_2Se_3$ that are separated by the $[Cd_2Br_4Se]^{2-}{}_\infty$ subunits. Although the Br is introduced, the calculation shows that it does not contribute to the VBT. This may be due to the elongated Sb–Br bonds and thus weak interaction between the $[Sb_4Se_5]^{2+}{}_\infty$ and other elements around it. The VBs of $Sb_2Se_3$ include the lone-pair electrons of the $Sb^{3+}$ ions, which result in antibonding interactions with those of the surrounding $Se^{2-}$ ions, and in turn, the CBs by the Sb–Se antibonding levels.

To understand why the band gap difference between $Bi_2Se_3$ and $InBi_2Se_4Br$ ($\Delta E_g = 0.91$ eV) is much bigger than that between $Sb_2Se_3$ and $CdSb_2Se_3Br_2$ ($\Delta E_g = 0.29$ eV), we have compared the band gaps of the binary compounds $Sb_2Se_3$ and $Bi_2Se_3$. From the EHTB calculations, the electronic structures of two compounds are similar. When relativistic effects are considered,[22] the calculated band gaps (originated from the 6s–4p interaction) of $Bi_2Se_3$ are conceivably smaller than $Sb_2Se_3$ (originated from the 5s–4p interaction). This is consistent with the observed band gaps 1.11 eV for $Sb_2Se_3$ and 0.3 eV for $Bi_2Se_3$. On the basis of the tight-binding calculation model, the orbital interaction is effected not only by the energy levels of orbitals but also the interaction of the electron cloud around the atoms, which could be described by the Slater-type orbital expansion.[18] In both binary phases, the building blocks, $[M_2Q_3]$ slabs, are similar but the interslab interaction in $Bi_2Se_3$ (shown in Figure S4 in the Supporting Information) is greater than those in $Sb_2Se_3$. Therefore, the resulting CB and VB are more dispersive in $Bi_2Se_3$ than in $Sb_2Se_3$, which accounts for the large difference in band gaps. The same is true in hybrid solids, where interslab interactions are missing; the band gaps of the Sb and Bi hybrids are thus comparable, while the difference between binary and hybrid solids for the Bi analogues is bigger.

For the band structure comparison between $CdSb_2Se_3Br$ and $InBi_2Se_4Br$, the chalcohalide spacer between the $[M_4Se_5]^{2+}_\infty$ sublattices, as suggested by the EHTB calculations, has effectively reduced the interaction between $[M_2Se_3]$ slabs, subsequently, to give the much less dispersive CB and VB. Also, both the Cd–Br and Cd–Se bonding levels lie much lower in energy than the Sb–Se bonding level. As a result, the band gap of $InBi_2Se_4Br$ is significantly increased compared to the band gap of $Bi_2Se_3$.

In summary, the origin of the band gaps is attributed to the absorption of energy for electrons populated in the bands almost exclusively made of the Sb–Se interactions. This is apparently true for the indium derivatives as well, because their structures are composed of the same $[M_4Q_5]^{2+}_\infty$ sublattices. Therefore, they have comparable band gap energies with binary chalcogenides, with the exception of the Bi-containing phases. The observed band gaps of the title series are wider than those of the corresponding $M_2Q_3$ binary phases. The blue shift can be explained by the QCE, a well-documented phenomenon that has been observed in other hybrid semiconductors.[23]

## Conclusions

Employing the concept of mixed-anion frameworks in synthesis, a new family of chalcohalide semiconductors was synthesized by conventional solid-state reactions at the intermediate temperature range. The investigation of this new series of chalcohalide compounds represents the first systematic study, as far as we know, among inorganic mixed-anion compounds reported thus far, showing the QCE on the optical band gaps. The UV–vis spectra indicate that these solids are midrange semiconductors, with the band gap of 1.3–1.8 eV, which exhibit a blue shift with respect to the corresponding $M_2Q_3$ binary phase. Because of reduced dimensionality, the less diverse orbital overlap results in narrower distribution of LUMO (CB) and HOMO (VB). Therefore, it gives rise to a further separation of CB and VB, consequently broadening band gaps.

**Acknowledgment.** Financial support for this research (DMR-0322905 and 0706426) and the purchase of a single-crystal X-ray diffractometer (CHE-9808165) from the National Science Foundation is gratefully acknowledged. L.W. is indebt to Prof. M.-H. Whangbo for offering training in the EHTB calculations.

**Supporting Information Available:** Parameters for extended Hückel tight-binding calculations, anisotropic thermal parameters, selected bond distances and angles for **1** and **4**, plots of the total and partial density of states calculated for $Sb_2Se_3$, PXRD and DTA plots, and X-ray crystallographic file, in CIF format. This material is available free of charge via the Internet at http://pubs.acs.org.

CM701995D

(22) Pitzer, K. S. *Acc. Chem. Res.* **1979**, *12*, 271–276.

(23) (a) Fu, H.; Zunger, A. *Phys. Rev. B: Condens. Matter Mater. Phys.* **1998**, *57*, R15064–R15067. (b) Axtell, E. A., III; Park, Y.; Chondroudis, K.; Kanatzidis, M. G. *J. Am. Chem. Soc.* **1998**, *120*, 124–136. (c) Axtell, E. A., III; Liao, J.-H.; Pikramenou, Z.; Kanatzidis, M. G. *Chem.—Eur. J.* **1996**, *2*, 656–666.